SAND2007-5397C
Proceedings of IMECE2007
2007 ASME International Mechanical Engineering Congress and Exposition
November 11-15, 2007, Seattle, Washington, USA

IMECE2007-41905

VALIDATION OF A NEW ALUMINUM HONEYCOMB CRUSH MODEL WITH DYNAMIC IMPACT TESTS

Terry Hinnerichs, William Scherzinger, Mike Neilsen, Tom Carne, and Eric Stasiunas
[1]Sandia National Laboratories
Albuquerque, NM 87185-0372

and

Wei-Yang Lu
[1]Sandia National Laboratories
Livermore, CA 94551-0969

ABSTRACT

This paper describes a process for validating a new constitutive model for large, high strain-rate deformation of aluminum honeycomb, called the Honeycomb Crush Model (HCM). This model has 6 yield surfaces that are coupled to account for the orthotropic behavior of the cellular honeycomb being crushed on-axis and off-axis. The HCM has been implemented in the transient dynamic Presto finite element code for dynamic impact simulations. The HCM constitutive parameters were identified based on Presto finite element models that were used to simulate uniaxial and biaxial crush tests of 38 lb/ft^3 aluminum honeycomb and reported in an earlier paper. This paper focuses on validating the HCM in the Presto code for application to impact situations that have honeycomb crush velocities up to 85 ft/sec. Also, a new approach for incorporating rate sensitivity into the model is described. A two-stage energy absorber with integrated aluminum honeycomb is described as the configuration for dynamic impact validation experiments. The test parameters and finite element model will be described along with the uncertainty quantification that was done and propagated through the model. Finally, correlation of model predictions and test results will be presented using an energy based validation metric.

INTRODUCTION

Aluminum honeycomb is an excellent shock mitigation material for vehicle bumpers or shipping containers. Its shock mitigation is enabled by its ability to convert kinetic energy of an impact into heat energy via large plastic deformation of the aluminum honeycomb structure. It is generally orthotropic with three principal material directions that result due to its composition of corrugated and flat aluminum sheets as shown in Figure 1. The principal material directions are: T-the strongest, L-the intermediate strength, and W-the weakest, as labeled in Figure 1.

Earlier papers [1-8] described a new constitutive model and its validation for representing the quasi-static large deformation crush of aluminum honeycomb. The new constitutive model, called the Honeycomb Crush Model (HCM) was aimed at improving the ability to predict off-axis, dynamic crush of aluminum honeycomb. The HCM has been implemented in the transient dynamic Presto finite element code [9] for dynamic impact simulations. HCM constitutive parameters were identified based on Presto finite element models that were used to simulate uniaxial and biaxial crush tests of 38 lb/ft^3 aluminum honeycomb, also reported in an earlier paper. This

[1] Sandia is a multiprogram laboratory operated by Sandia Corporation, a Lockheed Martin Company, for the United States Department of Energy's National Nuclear Security Administration under contract DE-AC04-94-AL85000.

paper focuses on validating the HCM in the Presto code for application to impact situations that have honeycomb crush velocities up to 85 ft/sec. First, the model validation space will be described. Next a summary will be given of how the dynamic crush test data was gathered and then compiled into results. A description will be given on how rate sensitivity is incorporated into the model and calibrated to uniaxial test data. The validation experiments will be described along with the finite element model and the uncertainty quantification that was done and propagated through the model. Finally, correlation of model predictions and test results will be presented using an energy-based validation metric.

Validation Space

In order to validate the honeycomb model, a validation space was identified that would encompass all the environments of the honeycomb for its design application. The validation space included: confinement of the honeycomb, segmented honeycomb orientation, angle of attack, impact angle, temperature, and velocity. The validation space diagram is shown in Figure 2. Colored areas on each validation axis represent parameters that were tested in the process of validating the honeycomb model. Each of the validation space axes are subsequently discussed in detail

The confinement criterion of the validation space, required by the design application of the honeycomb, was satisfied by the design of a two-layer aluminum shell structure that would confine the honeycomb within. Details of this shell structure are discussed in a subsequent section of this report.

Segmented honeycomb is a design concept which creates a cylindrical section of honeycomb that exhibits approximately the same crush strength in any radial direction. An example of segmented honeycomb can be seen in Figure 3. From the figure, it can be observed that the original honeycomb material has been cut into four 90^0 wedges and glued together so that the L-direction is approximately radial. For a lateral crushing impact on a cylindrical section of the segmented honeycomb, responses will differ depending on the exact orientation of the segmented honeycomb in relation to the impact. Therefore, the segmented honeycomb orientation was included in the validation space for testing and model prediction.

The angle of attack (AoA) is defined as the angle between the velocity vector of a structure and the axis of the structure itself, as shown in Figure 4. For validation experiments, two AoAs were applied to the honeycomb test structure—3^o and 20^o. A zero degree angle of attack was initially desired, but was not used for two experimental reasons: 1) An exact zero AoA would be almost impossible to obtain due to the orientation uncertainty of the test structure during testing. 2) In addition, the honeycomb would become extremely stiff with a zero AoA, possibly resulting in overloaded accelerometers. Therefore, a 3^o AoA was deemed a reasonable compromise that would reduce the potential problems associated with a zero AoA. The 20^o AoA was chosen for experimentation because it slightly exceeds the impact condition of the honeycomb in its real world application.

The impact angle is defined as the angle between the axis of the structure and the target surface. As shown in Figure 4, the impact angles are the complement of the AoA, or 87^o and 70^o, respectively. Previous material model testing with various impact angles have already been performed and are discussed in [1] and [2].

The temperature of the honeycomb material was varied for the validation experiments as specified in the validation space. Room temperature (77°F) and 165°F were the two variations of temperature used. The temperature, 165°F, was selected from the specifications of the real-world application of the honeycomb material.

The last validation space criterion, velocity, is defined as the impact velocity, or crush velocity, experienced by the honeycomb. The crush velocities used for the presented validation experiments ranged from approximately 0 ft/sec to 85 ft/sec. Quasi-static tests, performed in the lower range of the crush velocities (1 inch/min), provided a way to obtain quality data of the honeycomb crush through more precise instrumentation. Dynamic high-speed tests, with impact velocities reaching 85 feet/sec, were performed so that experimental data could be obtained near the maximum application velocity of the honeycomb, which was 150 feet/sec. Impact speeds above 85 ft/sec were unobtainable due to experimental facility limitations.

Experimentally Determined Rate Sensitivity of the Honeycomb

The rate sensitivity of the 38 lb/ft^3 aluminum honeycomb was quantified with three different testing techniques [7]. The first technique was designed for low crush rates from quasi-static up to 160 in/sec; the honeycomb was crushed at a constant rate using a high speed material test machine. Figure 5 shows data gathered with this technique at approximately 160 in/sec. Average crush strength for 160 in/sec and other test velocity data gathered with this first technique is given in Table 1.

The second technique [7] was a transient dynamic test designed to measure crush strength at the intermediate rates (0 to 600 in/sec). The transient nature of this technique provided data with varying crush velocity during the test. Consequently, the crush force had to be related to the instantaneous crush rate. This second technique did produce results down to quasi-static rates, overlapping the range covered by the first technique. The results from the two techniques compared well, providing confidence in both techniques. The test fixture was similar to that used for the low rate testing, consisting of a cylinder and a piston. However, in this fixture the load cell or force transducer was incorporated into the fixture, directly beneath the honeycomb, so that it measured the force applied to the

honeycomb. To create the transient crush force, the entire test fixture, consisting of the cylinder, piston, honeycomb sample, and integral force transducer, was mounted on the carriage of a standard drop table and accelerated to a speed of approximately 600 in/sec. before impacting an inertial mass. Figure 6 shows this data as a function of crush velocity. The red line present in the data is a linear least-square fit to the measured data, and is defined in Eq. 1, where the crush strength is in ksi and the crush velocity is in ft/sec.

$$\sigma_{crush} = 6.1 + 1.45 * 10^{-2} * V_{crush} \qquad \text{Eq. 1}$$

The third technique [7] also measured the crush strength at intermediate rates by utilizing a compressed air actuator which propelled a loading mass and the honeycomb sample into an inertial mass. For this technique, no constraining fixture was included with the honeycomb sample in order to reduce the test complications and the overall test mass. Instead, a cylindrical section of honeycomb was radially confined by wrapping the cylinder with fiber-reinforced tape. This technique for confinement had been previously evaluated and shown to produce equivalent results to those of the cylinder-piston confining fixture [10]. Due to the highly oscillatory nature of the crush strengths versus velocity for these tests only the crush strength and mean velocity are given in Table 2.

The data from all three techniques can also be compared using the linear best-fit relationship derived from the data from Technique Two. Figure 7 shows the linear relationship, plotted in blue using a log scale for the crush rate, with results from Techniques One and Three overlaid on the graph. Of course, the linear relation does not appear to be a straight line using the log scale for the crush rate. Included with the blue linear relationship are two dash-dot curves showing the 95% confidence bounds for this estimation of the mean crush stress. The results from the first technique are represented by their mean values with vertical uncertainty bars at the four crush rates, rather than including all the individual sample data as in Figure 7. The results with Technique Three are indicated with asterisks, having large uncertainty.

Rate Sensitivity of the Honeycomb Crush Model

The HCM model, as previously reported [8], has calibrated crush strength functions for each normal and shear stress component. The incorporation of rate sensitivity into the crush strength of the HCM was based on the observation that an initial peak in the crush stress always exists during quasi-static or dynamic crushing of the honeycomb; e.g. see Figure 5. Including an initial peak crush stress results in a realistic rate sensitivity predicted by the model. Graphically, this initial peak function which is part to the model definition is shown in Figure 8.

This peak is associated with the buckling/collapse process of crushing each row of unit cells in the cellular honeycomb structure as shown in Figure 9a. Figure 9b shows a similar deformation pattern predicted by the HCM operating in the Presto code with the same uniaxial loading. Here the blue elements are undeformed honeycomb and the red elements show the crush front propagating through the model from bottom to top in this case. The light blue element represents the transition zone.

Figure 10 shows the crush strength versus volumetric strain that the HCM predicts given the crush strength function shown in Figure 8. Notice how the crush strength peak repeats itself as each row of finite elements crush which is similar again to what is observed in the test data as shown in Figure 5. Consequently, the size of a finite element effectively creates a length scale that can be used to factor in the physical unit cell size of the honeycomb which is 0.125 inch for this 38 lb/ft^3 honeycomb. Choosing an element size equivalent to the honeycomb unit cell size enables a similar deformation pattern to what occurs in the physical hardware.

The rate sensitivity of the HCM as a function of the shape of the initial peak in the crush strength function, as shown in Figure 8, was examined. The magnitude of the peak, duration of the peak, and element size were varied while simulating a crush velocity of 1000 in/sec. Duration of the peak and element sizes were varied from 0.5 to 2 times the baseline values. Negligible change in rate sensitivity of the HCM resulted. However, there was significant sensitivity to the height of the peak as shown in Figure 11. The value of 1.3 was selected for the normalized height of the initial peak that calibrates with the available dynamic crush data.

A comparison of the HCM's rate sensitivity to the test data from the three testing techniques is shown in Figure 12 which is basically a re-plot of Figure 7 with the HCM model predictions. The superimposed blue line is the nominal curve, and the dashed lines are the +/- 10% values. Here, the red curve represents Eq. 1 or the linear regression fit to data from the second testing technique. The red symbols are the test data groupings from Techniques One and Three.

Honeycomb Constitutive Model and Propagation of Uncertainty

Similar to the quasi-static validation process applied in [8], two categories of model parameters will be treated as random variables with uncertainty bands and propagated through the model, as listed in Table 3. The first category contains the six initial yield stress values with their estimated maximum and minimum values. These values are primarily based on the quasi-static calibration and validation process previously performed [8]. However, the calibration for the TS parameter was weighted more towards the high strain rate data reported in Figure 7, which resulted in the value of 6100 psi. Also, the +/- 10% range was chosen to factor in the variation of crush strength from sample-to-sample, temperature changes, and segmenting the honeycomb. Crush test data have shown sample-

to-sample variation in T-crush strength is about 5%, changing the temperature from ambient to 165 F is minus 10%, and crush tests on segmented honeycomb have shown it to be up to 5% stronger than regular aluminum honeycomb [6].

The second category is the coefficient for Coulomb friction, or the level of friction between the honeycomb and the container and between the container contacting itself. The lower coefficient of friction bound of 0.2 is based on friction measurements with lubricated aluminum surfaces [11]. The upper coefficient of friction bound value of 1.0 is based on dry static friction of aluminum on aluminum [12].

Validation Experiments

The validation space was used for the design of the honeycomb validation experiments, as shown in the test matrix of Table 4. The first column lists the configuration of the honeycomb material, which will be described in subsequent paragraphs. The next column lists the temperature of the honeycomb material for that particular test series; T_o refers to ambient temperature tests. Three test samples, or units, were used for each configuration as indicated by the next column. The last column lists the names of the test series and samples.

Confinement of the honeycomb material was used for the majority of the validation space testing. In an effort to confine the honeycomb and represent the system application, a two-layer test structure, also referred to as a two-layer cake (TLC), was designed and is shown in Figure 13. The TLC configuration consisted of placing two circular honeycomb samples of different diameters and orientations into an aluminum shell, one on top of the other. The top layer was segmented. The bottom layer of honeycomb was uniform material, oriented with the honeycomb's T-direction aligned in the axial direction of the TLC and the L-direction running parallel with the TLC's plane of symmetry. A thin load spreader plate with a nominal thickness of 0.025 inches separated the two layers of honeycomb material. The nominal wall thickness of the 6061-T6 aluminum shell was 0.035 inches and the diameters for the top and bottom were 3 inches and 4 inches, respectively. Once assembled, the TLC structure provided confinement to the honeycomb with the characteristics of the system application.

The orientation of the segmented honeycomb in the top layer of the TLC structure was varied for the quasi-static tests and remained constant for the dynamic tests. This orientation, defined as X or +, is determined by what point on the segmented honeycomb first comes into contact with the target for the 3^o and 20^o AoA test conditions. If the target initially contacts the honeycomb directly in between the glue joints, then this is considered an X orientation. Alternately, if the target initially contacts the honeycomb at a glue joint, this is considered a + orientation. A diagram illustrating the X-orientation can be seen in Figure 14. Rotating the honeycomb sample 45 degrees relative to the loading vectors in Figure 14 results in the + configuration.

Validation Metric

One measure of how appropriate a model is for a shock mitigation device is its ability to predict the amount of energy absorbed by the device during an impact. For this reason, the metric chosen for determining the goodness of fit between model and test data will be based on absorber energy. The validation metric is given by Equation 2.

$$E = \int_0^{\delta_{\max}} F \bullet d\delta \qquad \text{Eq. 2}$$

where F is the crush force applied to the test structure in the loading or axial direction, and $\delta_{\max}$ is the maximum crush distance. Equation 2 is an integral measure that will factor in the general shape and the area under the force versus displacement curves. This energy metric is used to compare energy absorbed in the model with the test data. Being an integral measure, it smoothes the model data and test data, making it easier to compare the two as well as being more relevant to the system application.

Finite Element Model of the Two Layer Cake

An undeformed cross-section of the finite element mesh for the 3^o AoA impact is shown in Figure 15a. The deformed shape of the mesh 3 msec into the impact is shown in Figure 15b. The elements simulating the 38 lb/ft^3 aluminum honeycomb were given the size of 0.125 in. to match the unit cell size for this honeycomb. A total of 21,000 eight -node hexahedral elements were used in the model with one plane of symmetry used to cut the model size in half.

The TLC without honeycomb inside will be referred to as the "empty-can". The 6061-T6 aluminum in the empty-can was modeled with a Power Law Hardening elastic-plastic Von Mises constitutive model with: Young's modulus of 9.9e6 psi, Poisson's ratio of 0.33, initial yield stress of 40.e3 psi, hardening coefficient of 27.e3 psi, hardening exponent of 0.42, and no cracking allowed. However, in the experimental tests, cracking did occur in the TLC and the empty can. The modeling error associated with ignoring cracking will be discussed later. Finally, the Impact Mass and Inertial Mass are steel blocks weighing 107 and 8000 lbs., respectively.

An undeformed cross-section of the finite element mesh for the 20^o AoA impact is shown in Figure 16a. The deformed shape of the mesh 3 msec into the impact is shown in Figure 16b. The Impact and Inertial masses used here were the same as for the previous 3^o AoA impact.

Model Predictions of Empty and Filled Two Layer Cake

Presto and the HCM were used to predict the response of the TLC during the 3° and 20° AoA impact tests. The 3° impact test was simulated with an initial velocity of 85 ft/sec. and the 20° impact test with an initial velocity of 69 ft/sec, which were the actual speeds used during experimental testing. These initial velocities and the upper and lower bounds for the strength values and friction values tabulated in Table 3 were used in the Presto and HCM predictions. Also, a simulation was done of the crush of the empty-can (TLC without the honeycomb) using an initial velocity of 3.3 ft/sec to approximate a quasi-static crush experiment.

Figure 17 shows the HCM predictions of crush force versus crush distance for the 3° AoA impact configuration. Crush distance is the amount that the TLC is compressed during the impact. The four highest curves show the four combinations of the strength and friction values propagated through the model. The "High" term in the legend refers to the highest values for the strength parameters and the "Low" term refers to the lowest. The "mu" refers to the coefficient of friction. Notice that there are two crush force plateaus. The first plateau relates to the crushing of only the first layer. The second plateau has a higher force level because the second layer is now being crushed, and it supports a higher force due to its larger diameter. The lowest, or cyan, curve is the predicted crush force for the empty-can. These results imply that the empty-can may support approximately 10% of the crush force for the 3° AoA impact.

Figure 18 shows the HCM predictions for the 3° AoA impact in terms of the energy metric. The most energy is absorbed for the prediction with "High" strength and high friction (mu=1.0). The least energy is absorbed for "Low" strength and low friction (mu=0.2). These two upper/lower bounding curves will be used later as an estimate for the model's 95% confidence interval to correlate with test data as part of the model validation process. The empty-can results imply that the can may absorb approximately 10% of the energy.

Figure 19 shows the HCM predictions of crush force versus crush distance for the 20° AoA impact configuration. The influence of honeycomb strength and friction levels is given for the full TLC model in the four upper curves. The large oscillations in the curves are due to the collapse of individual element rows in the model. This may also be the cause of oscillations observed in the test data shown later. The lower or cyan curve is for the empty-can crush results.

Figure 20 shows the HCM predictions for the 20° AoA impact in terms of the energy metric. Similar to the 3° AoA impact, the most energy is absorbed for the case with "High" strength and high friction (mu=1.0). The least energy is absorber for "Low" strength and low friction (mu=0.2). These two upper/lower bounding curves will be used later, again as an estimate of the model's 95% confidence interval to correlate with test data as part of the model validation process. The cyan curve or empty-can results imply that the can may absorb approximately 10% of the energy.

Direct Correlation of Model Predictions with Test Data and Uncertainty

Figure 21 shows the upper and lower bound model predictions for the crush force versus crush distance for the 3° AoA impact compared to test data. The test data include curves from tests at ambient (R tests) and 165° F (S tests) temperatures. Very little difference exists in the test data between the two temperatures. The most striking feature of the plot is the large oscillations in the test data but not in the model. No apparent vibration mode for this oscillation was found in the load train of the TLC. However, the model appears to envelope the mean value of the test data quite well which will be quantified better with the energy metric in the next figure.

Also, model prediction and test results for the empty-can crush are given in Figure 21 in the lower force range of the figure. The explicit Presto model simulated an empty-can crush of 20 in/sec for computational efficiency whereas the test was done at 0.017 in/sec. The higher speed model simulation over-predicts the crush force for the empty-can compared to the quasi-static test data. How much of this over-prediction is correct due to the higher speed simulation is not known, especially since there are two other contributing reasons: 1) some cracking did occur in the test but was not included in the model and 2) only three hexahedral elements were used through the thickness for the thin walls of the empty-can, which tends to make the structure overly stiff. Consequently, the entire difference between model and test for the empty-can will be considered in the validation process later.

Figure 22 shows the upper and lower bound model predictions for the energy metric versus crush distance for the 3° AoA impact compared to test data. The test data include curves from tests at ambient (R tests) and 165° F (S tests) temperatures. Very little difference exists in the test data between the two temperatures so the two data sets were combined. The black dots indicate the 95% confidence intervals of the combined R and S tests at the 1/3, 2/3, and total energy points along the curve calculated using the probability interval expression for the true experimental crush energy, $\overline{CE}$ in Eq 3.

$$\overline{CE_e} - t_{\frac{\alpha}{2},v}\frac{s}{\sqrt{n}} < \overline{CE} < \overline{CE_e} + t_{\frac{\alpha}{2},v}\frac{s}{\sqrt{n}} \qquad \text{Eq. 3}$$

The procedure for calculating the 95% confidence interval (CI) for each test series requires the assumption that the data from each series is from a normal population. The sample crush energy mean estimate, $\overline{CE}_e$, and sample standard deviation, *s*, from 6 test samples (n=6) can then be calculated. For a 95%

CI, an α-value of 0.05 is used with $t_{\frac{\alpha}{2},\nu}$ and $\nu = n-1$ degrees-of-freedom to find the t-distribution value of 2.571. These values are combined in Eq. 3 to find the estimated mean with 95% CI. Details for this procedure can be found in [13].

The most desirable agreement between model and test would be for the model to envelope the 95% confidence interval of the test data and have the same mean as the true experimental data mean; thereby accounting for all the uncertainties in the test data, including material variability, friction, and temperature. Here the model does envelope the two highest energy confidence intervals but misses the lowest energy interval.

The true crush energy error with the computational model, E, is given in Eq. 4.

$$E = \overline{CE}_m - \overline{CE} \qquad \text{Eq. 4}$$

Here, $\overline{CE}_m$ is the crush energy mean value for the model at each of the three energy levels. It was calculated based on the average of the model's upper and lower bound values for each of the three energy levels. Since the true experimental mean, $\overline{CE}$, is not known, another validation metric or estimate of the error associated with the model is given in Eq 5.

$$\widetilde{E} = \overline{CE}_m - \overline{CE_e} \qquad \text{Eq. 5}$$

where $\overline{CE}_e$ is the estimated experimental mean value for the crush energy. Equations 3 , 4, and 5 can be manipulated into a probability interval expression for the model's true error, E, given in Eq. 6. Details are given in [14].

$$\widetilde{E} - t_{\frac{\alpha}{2},\nu}\frac{s}{\sqrt{n}} < E < \widetilde{E} + t_{\frac{\alpha}{2},\nu}\frac{s}{\sqrt{n}} \qquad \text{Eq. 6}$$

Table 5 shows the results from applying Equations 3-6 for each of the three energy levels to the 3° AoA impact model predictions and test results. The crush distance for each energy level is given. The 95% confidence interval for the mean experimental crush energy is given based on the inequality in Equation 3 followed by the mean crush energy predicted by the model. Notice that the mean crush energy predicted by the model is very close to the CI test interval, but only falls within it for the 3/3 E energy level. The last two lines in Table 5 are from the inequality in Equation 6 and give the 95% probability interval for the true model error. Note that the model error is less than 4% for the two highest energy levels but goes as high as 16% for the lowest energy level.

The energy curves of the empty-can crush for the model and test are also shown in Figure 22. One estimate for the error associated with the empty-can model is the difference between the empty-can model and test energy curves which is approximately 4 to 5% of the nominal model value. Even if this error estimate is subtracted from the TLC model predictions, they would still overlap the 95% confidence intervals for the test data at the upper two energy levels.

Figure 23 shows the upper and lower bound model predictions for the crush force versus crush distance for the 20° AoA impact compared to test data. The test data include curves from tests at ambient (T tests) and 165° F (U tests) temperatures. Similar to the 3° AoA data, very little difference exists in the test data between the two temperatures. The model versus test data for the empty can crush is given towards the bottom of the figure. The model's upper and lower predictions envelope the test data very well. Again, the two lower curves come from the model simulating an empty-can crush at 20 in/sec and the test was done at 0.017 in/sec.

Figure 24 shows the upper and lower bound model predictions for the energy metric versus crush distance for the 20° AoA impact compared to test data. The test data include curves from tests at ambient (T tests) and 165° F (U tests) temperatures. Very little difference exists in the test data between the two temperatures. The black dots indicate the 95% confidence intervals of the combined R and S tests at the 1/3, 2/3, and total energy points along the curve using Equation 3. Here the model does envelope the test data 95% confidence interval; thereby accounting for all the uncertainties in the test data for all three energy levels.

Table 6 shows the results from applying Equations 3 through 6 for each of the three energy levels to the 20° AoA impact model predictions and test results. The crush distance for each energy level is given. The 95% confidence interval for the mean experimental crush energy is given based on Equation 3, followed by the mean crush energy predicted by the model. Notice that the mean crush energy predicted by the model is very close to the CI test interval but only falls within it for the 3/3 E energy level. The last two rows in Table 6 are from Equation 6 and give the 95% probability interval for the true model error. Note that the model error is less than 4% for the two highest energy levels but goes as high as 16% for the lowest energy level.

The energy curves for the empty-can crush model and test are also shown at the bottom of Figure 24. Again, consider that the estimate for the error associated with the empty-can model is the difference between empty-can model and test energy curves. Even if this error estimate is subtracted from the TLC model predictions they would still overlap the 95% confidence intervals for the test data for all three energy levels.

The model is judged to have predictive value and be valid based on the observed amounts of overlap between the predicted envelope of crush energy and the 95% confidence interval for the test data for five of the six check points. Also, the model was judged to be valid based on the modeling error estimates being 10% or less for five of the six energy check points (two highest 3^o AoA and all three 20^o AoA). The model only failed to overlap the test data for the lowest energy level with the 3^o AoA impact and under-predicted the test in this case with a maximum modeling error of 16%.

Further work should include quantifying the additional crush strength of the segmented aluminum honeycomb due to the epoxy adhesive and adding more fidelity to the empty-can model in the form of a more refined finite element mesh and the ability to allow cracking to occur.

SUMMARY AND CONCLUSIONS

The process for validating the Honeycomb Crush Model (HCM) with dynamic crush data was presented. Uncertainty was propagated through the model in the form of the initial normal and shear strengths along with friction between the honeycomb and the two layer cake confinement structure. Test data for calibrating the rate sensitivity of the HCM were presented. A new approach for incorporating rate sensitivity in the model and the calibration with dynamic uniaxial test data was described. The validation tests involved crushing the two layer cake structure filled with 38 lbs/ft^3 aluminum honeycomb at speeds up to 85 ft/sec and with two angles-of-attack relative to the target.

Validation procedures included the effects of experimental and modeling uncertainty. Predictions using the calibrated HCM were compared with the validation test data using an energy metric to quantify the degree of agreement between model and test results.

The model was judged to be valid based on the observed amounts of overlap between the predicted envelope of crush energy and the 95% confidence interval for the test data for five of the six check points. Also, the model validation was based on the estimated modeling errors of 10% or less for five of the six energy level check points. The lowest energy point for the 3^o angle of attack displayed the largest modeling error of 8 to 16%.

Further work should include quantifying the additional crush strength of the segmented aluminum honeycomb due to the epoxy adhesive and adding more fidelity to the empty-can model in the form of a more refined finite element mesh and the ability to allow cracking to occur.

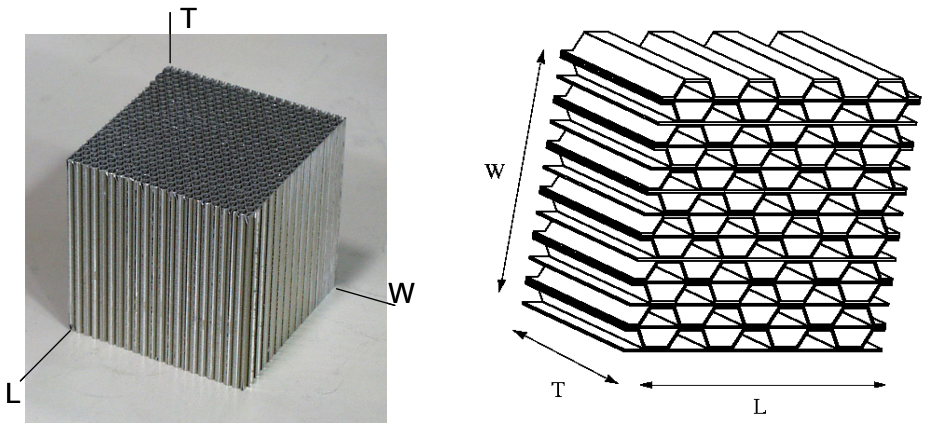

FIGURE 1. ALUMINUM HONEYCOMB GEOMETRY AND PRINCIPAL DIRECTIONS

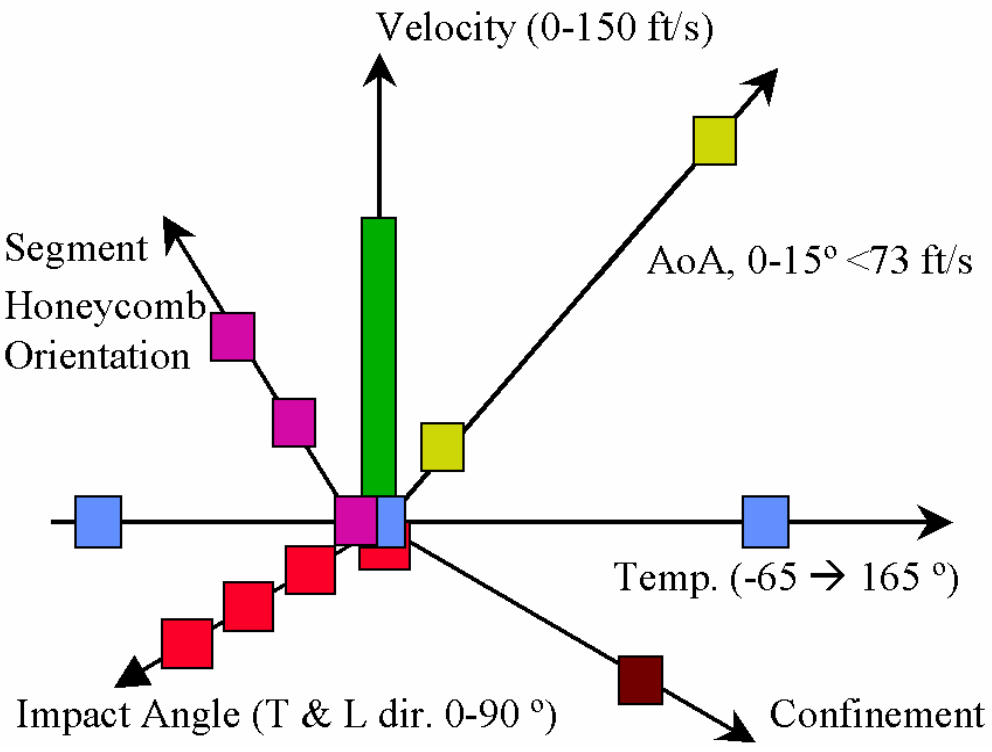

FIGURE 2. VALIDATION SPACE

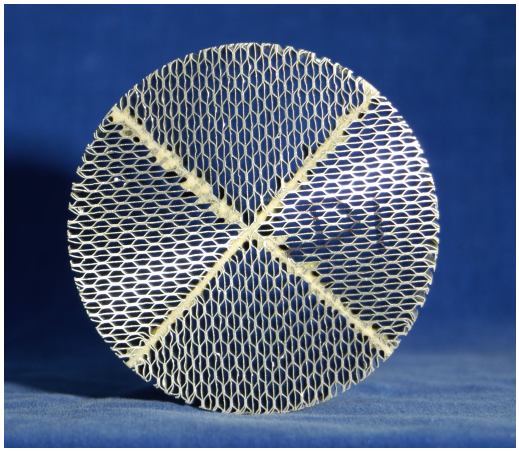

FIGURE 3. SEGMENTED HONEYCOMB

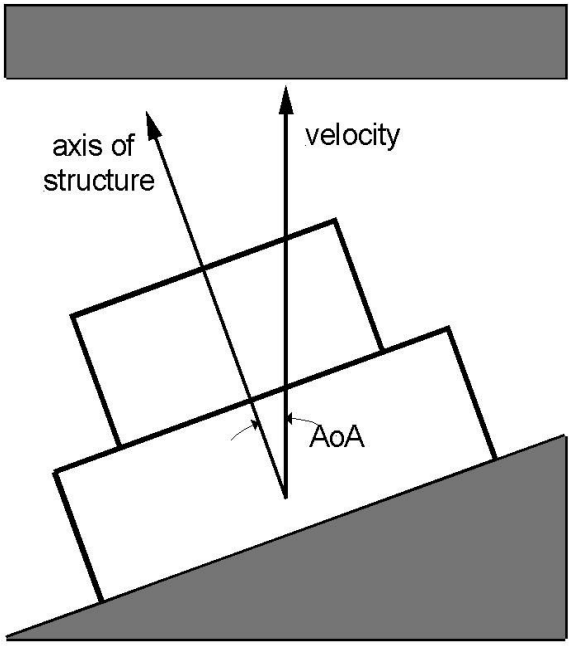

FIGURE 4. ANGLE OF ATTACK

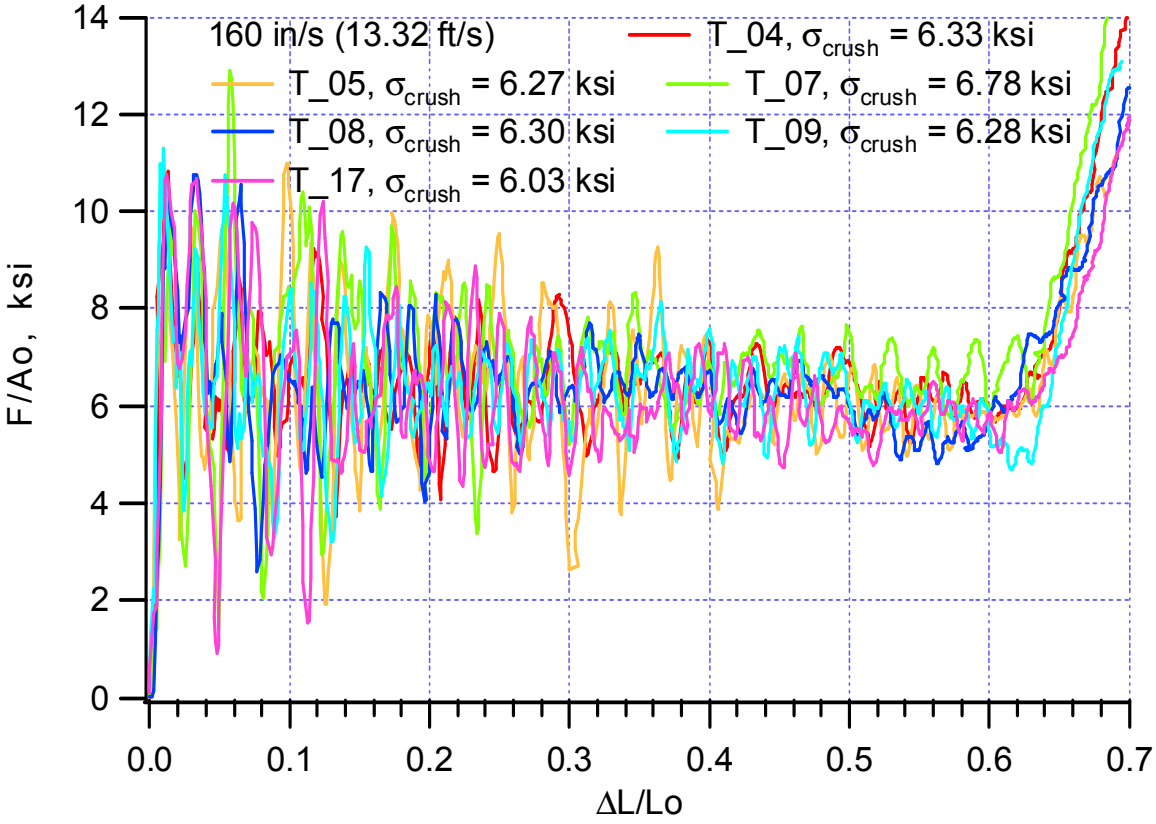

FIGURE 5. CRUSH TEST RESULTS FROM THE MATERIAL TESTING MACHINE, TECHNIQUE ONE

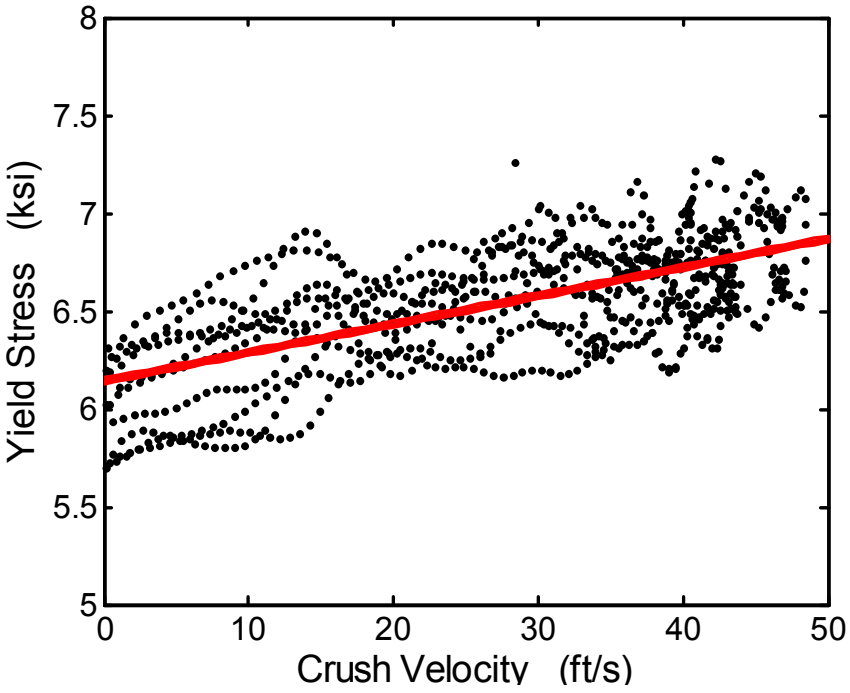

FIGURE 6. YIELD STRESS VERSUS CRUSH VELOCITY FOR TECHNIQUE TWO

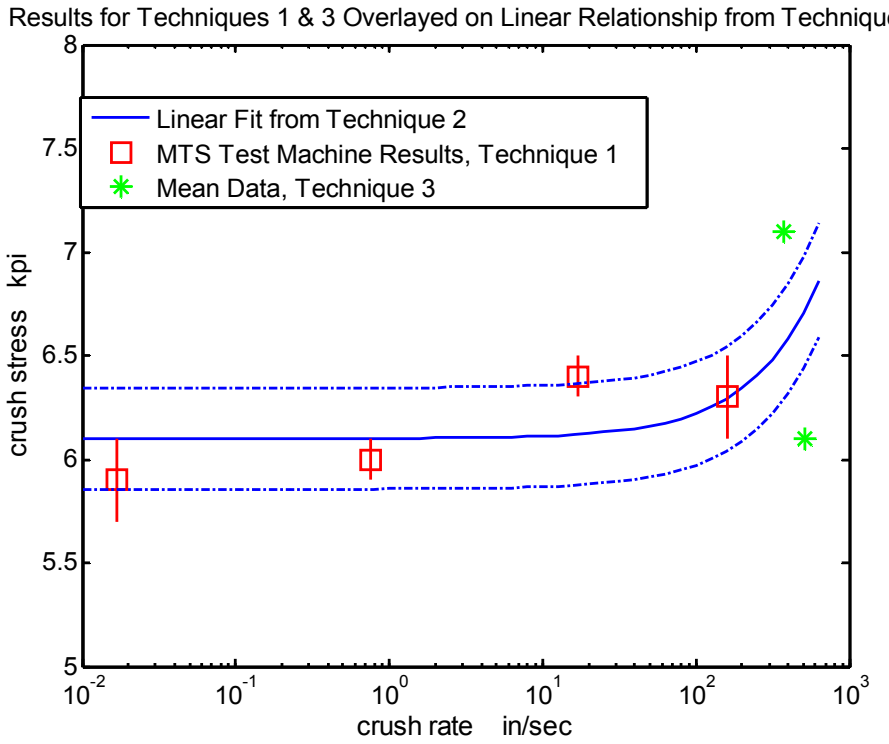

FIGURE 7. COMPOSITE PLOT OF CRUSH STRESS RESULTS FROM ALL THREE TESTING TECHNIQUES

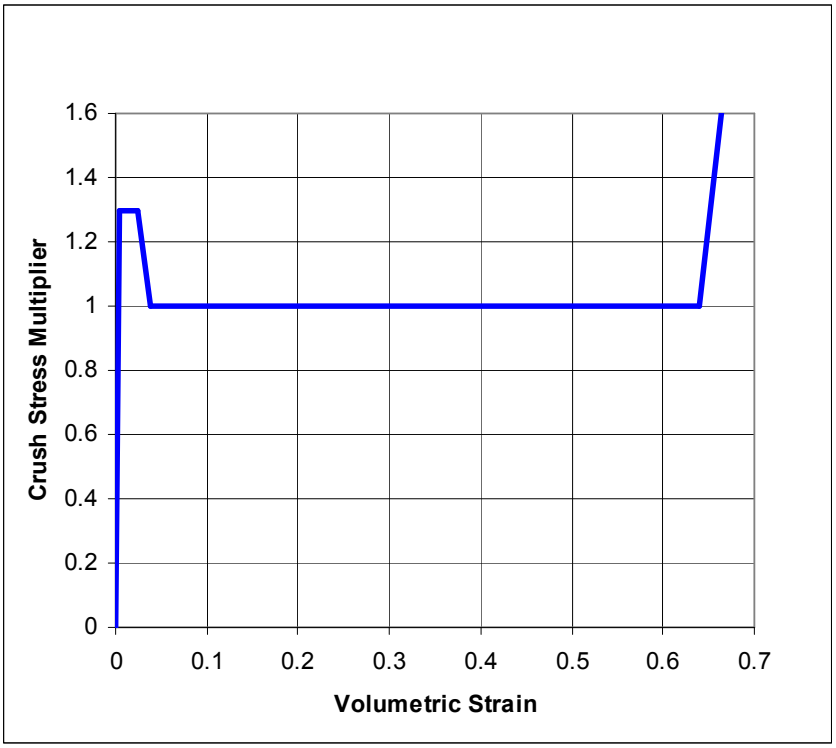

FIGURE 8. CRUSH STRESS VERSUS STRAIN VALUES INPUT TO THE HCM

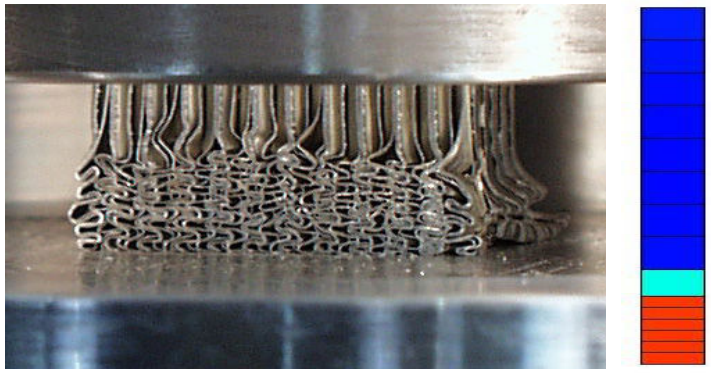

(a) (b)

FIGURE 9. COMPARISON OF CRUSH BEHAVIOR IN EXPERIMENT TO MODEL: (a) EXPERIMENT, (b) MODEL

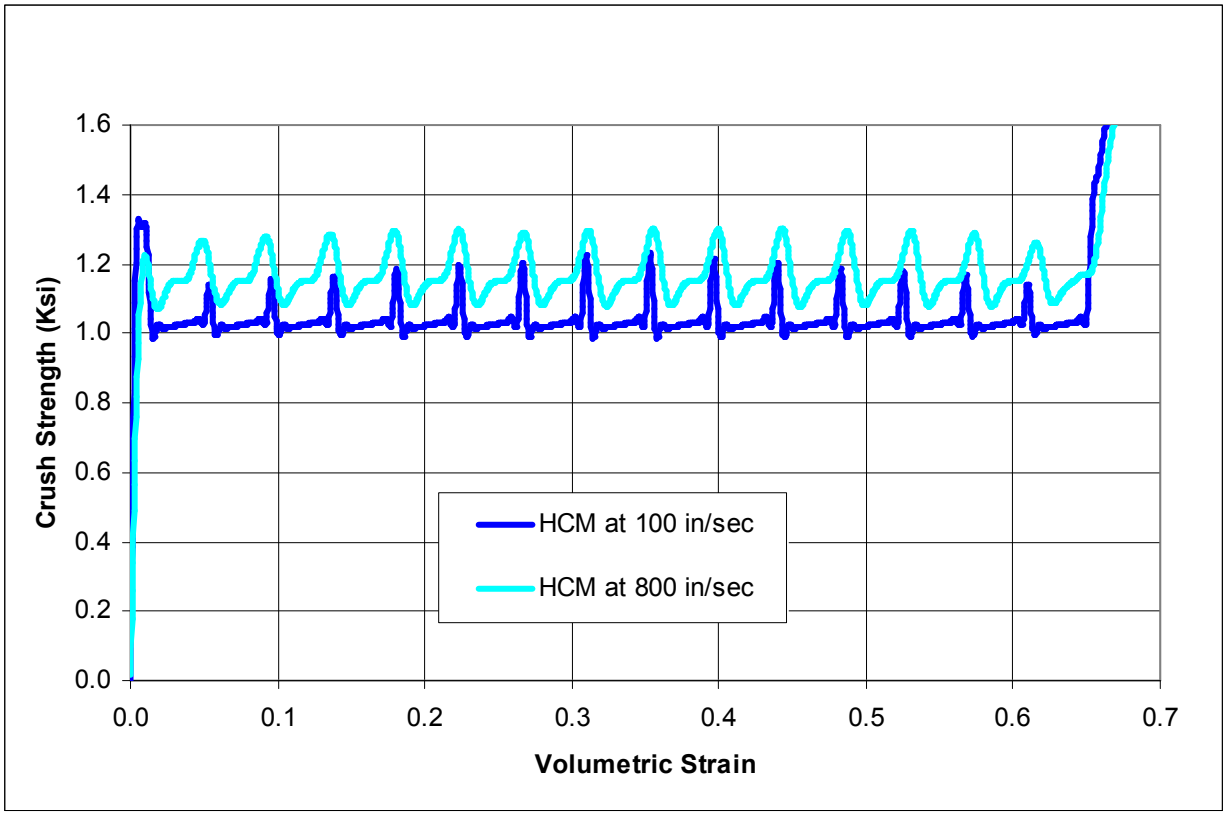

FIGURE 10. CRUSH STRENGTH VERSUS STRAIN PREDICTED BY THE HCM AT TWO IMPACT SPEEDS

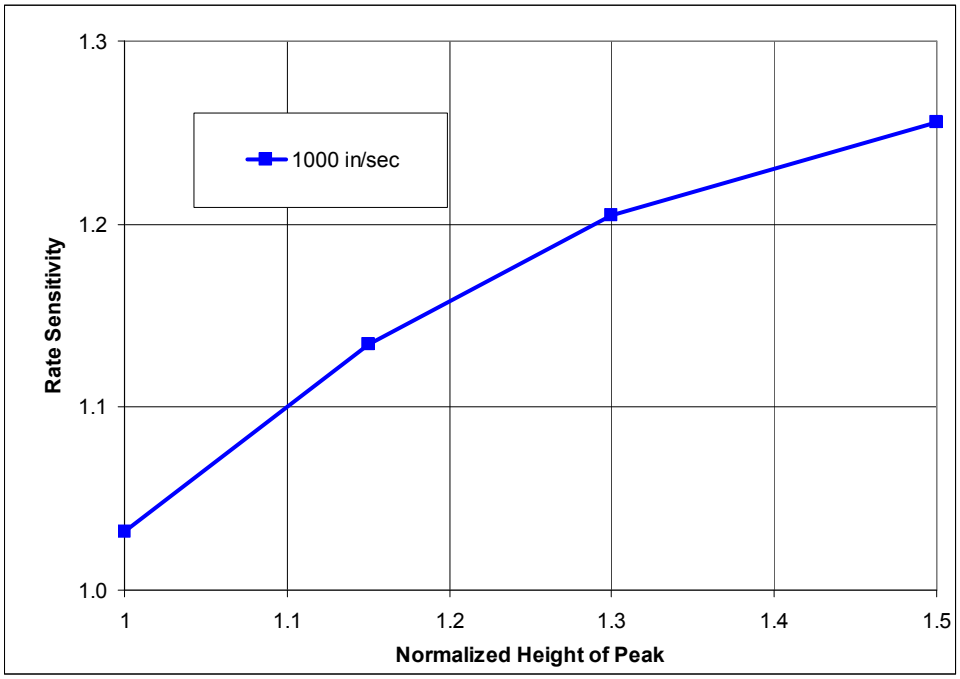

FIGURE 11. VARIATION OF THE HCM RATE SENSITIVITY DUE TO HEIGHT OF THE INITIAL CRUSH STRENGTH PEAK

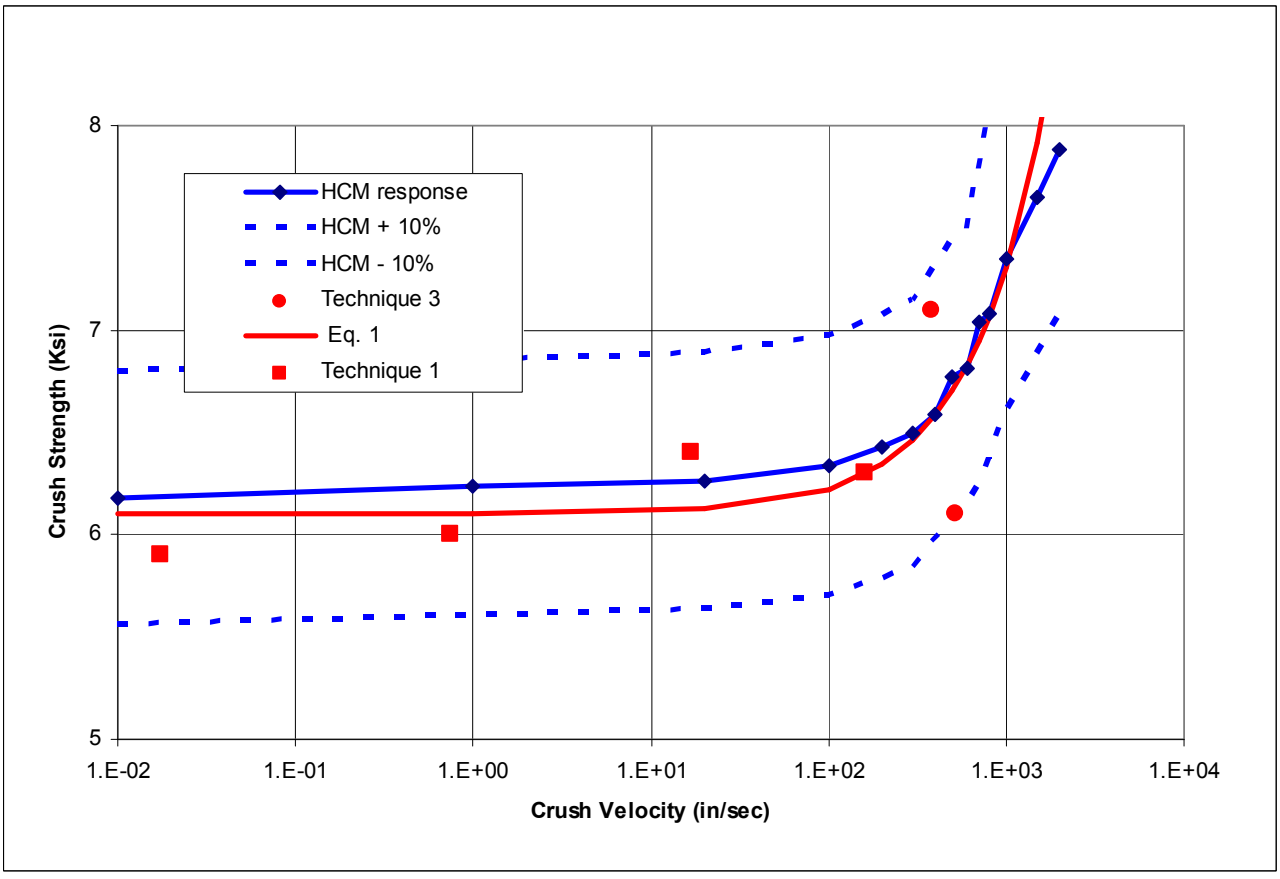

FIGURE 12. COMPARISON OF HCM RATE SENSITIVITY TO TEST DATA

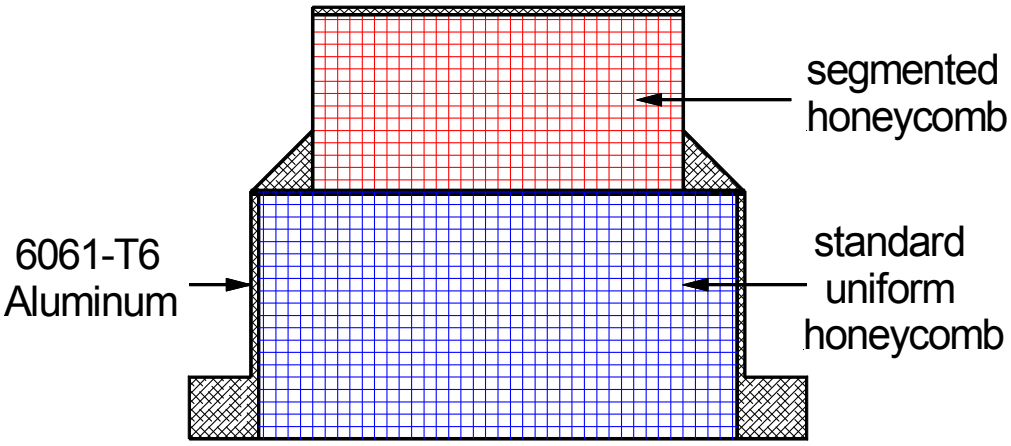

FIGURE 13. TWO-LAYER CAKE (TLC) CROSS-SECTION

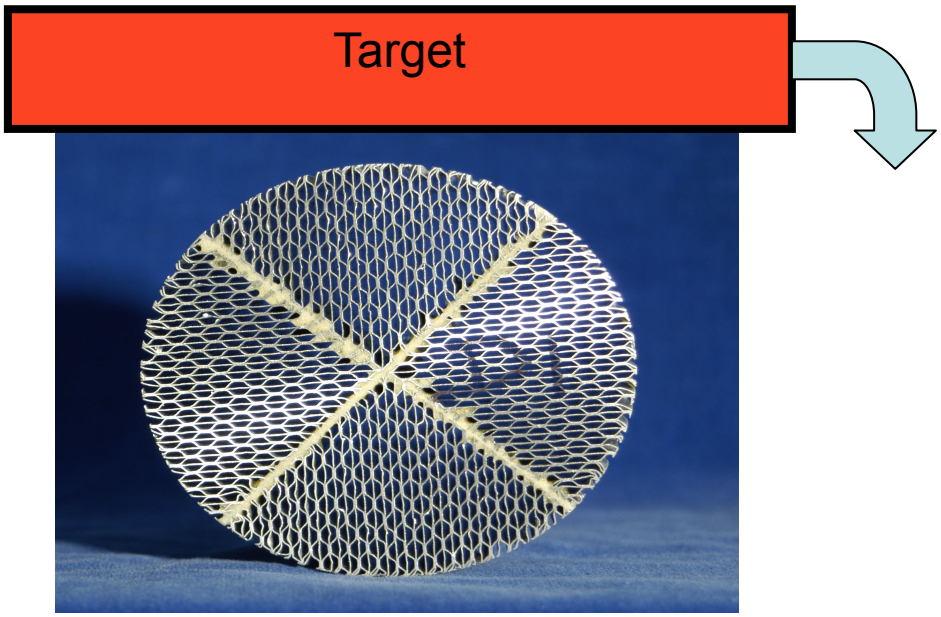

FIGURE 14. SEGMENTED HONEYCOMB IN THE X ORIENTATION

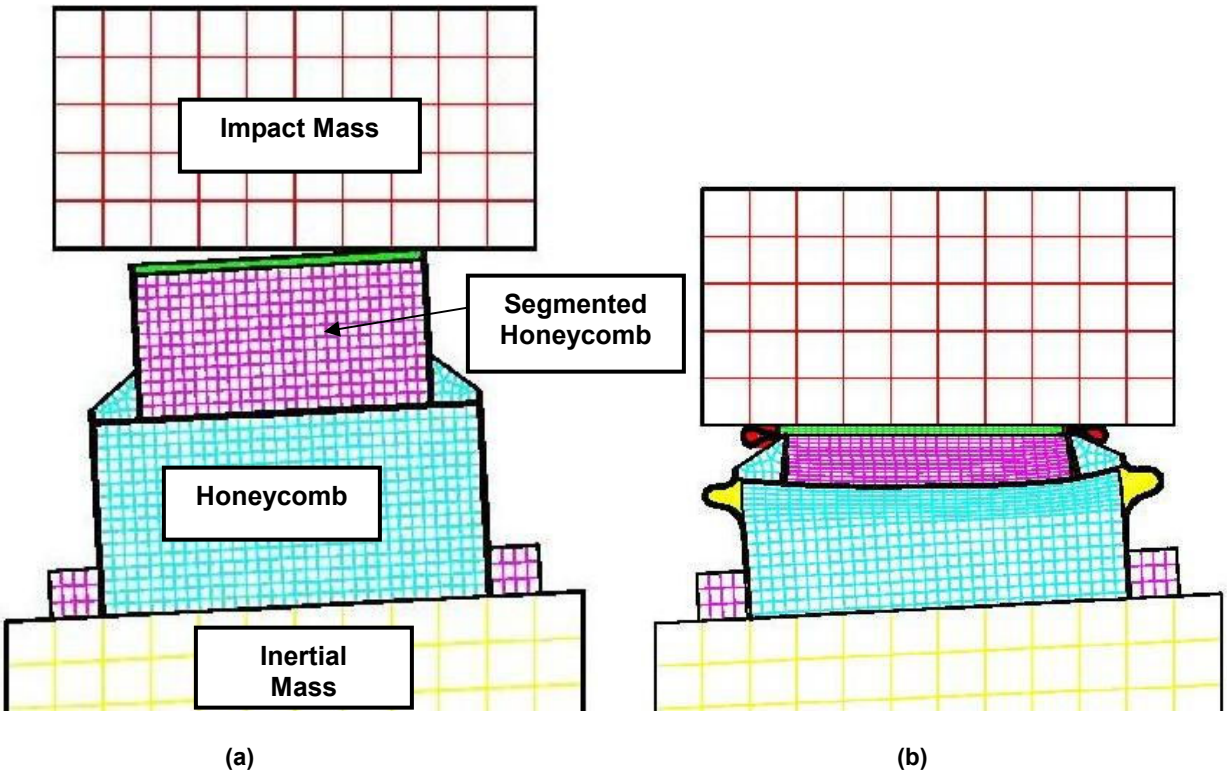

FIGURE 15. TWO-LAYER CAKE TEST ARTICLE WITH 3^{O} AOA: a) UNDEFORMED, b) AT TIME 3 MSEC INTO IMPACT

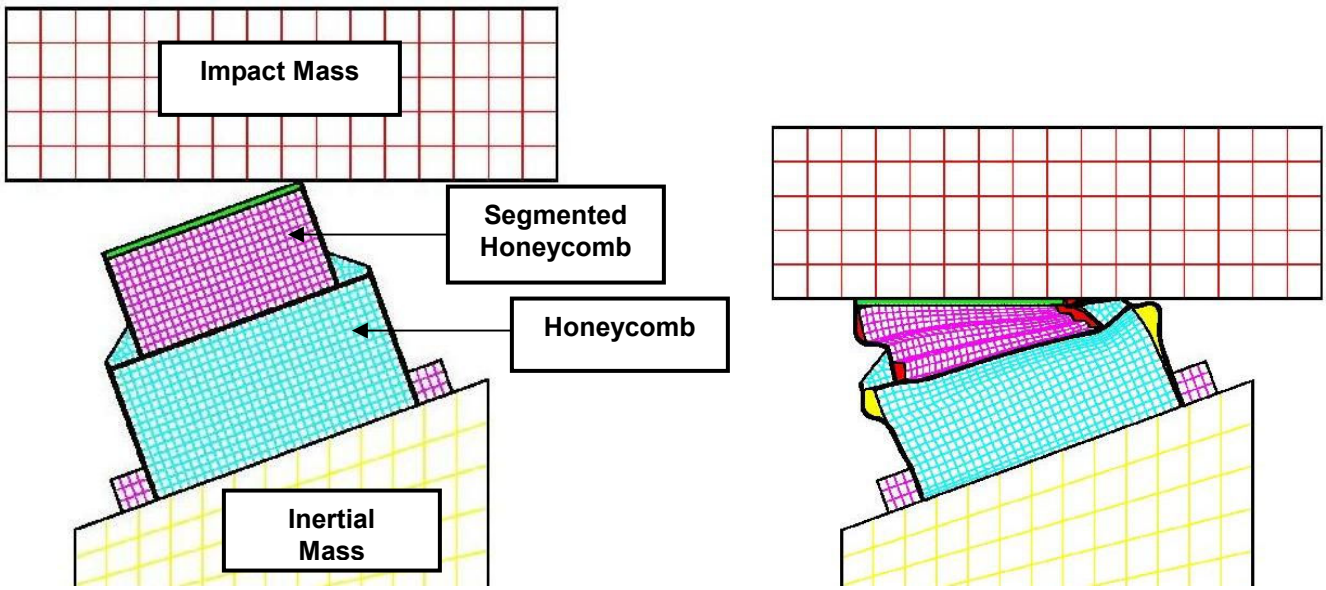

FIGURE 16. TWO-LAYER CAKE TEST ARTICLE WITH 20^{O} AOA: A) UNDEFORMED, B) AT TIME 3 MSEC INTO IMPACT

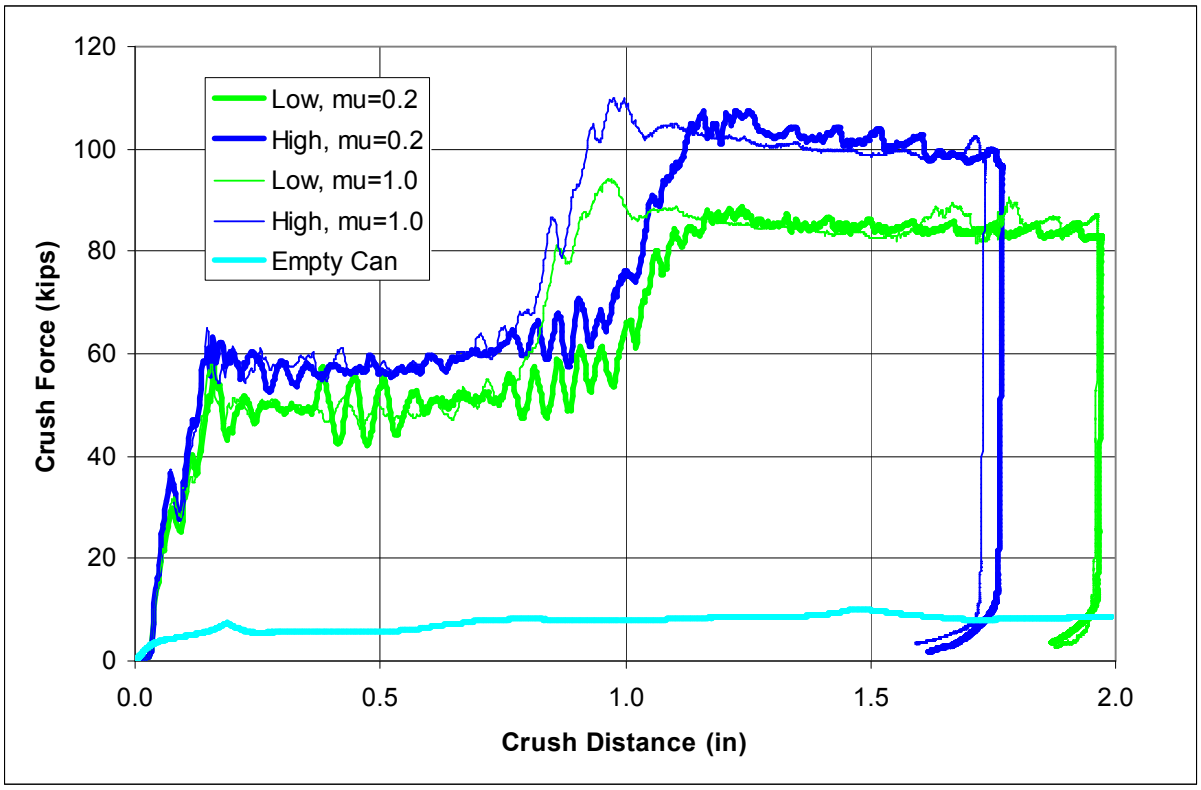

FIGURE 17. HCM PREDICTIONS OF CRUSH FORCE FOR 3^{O} AOA WITH STRENGTH AND FRICTION VARIABILITY

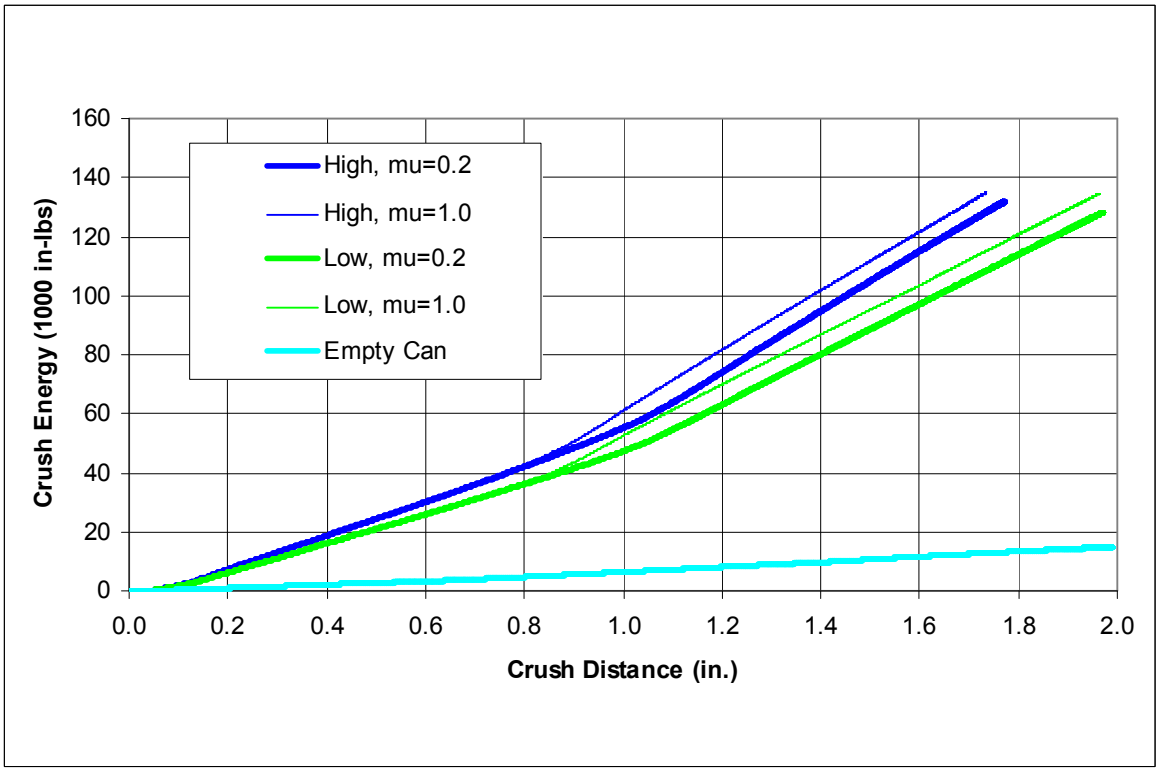

FIGURE 18. HCM PREDICTIONS OF ENERGY METRIC FOR 3^{O} AOA WITH STRENGTH AND FRICTION VARIABILITY

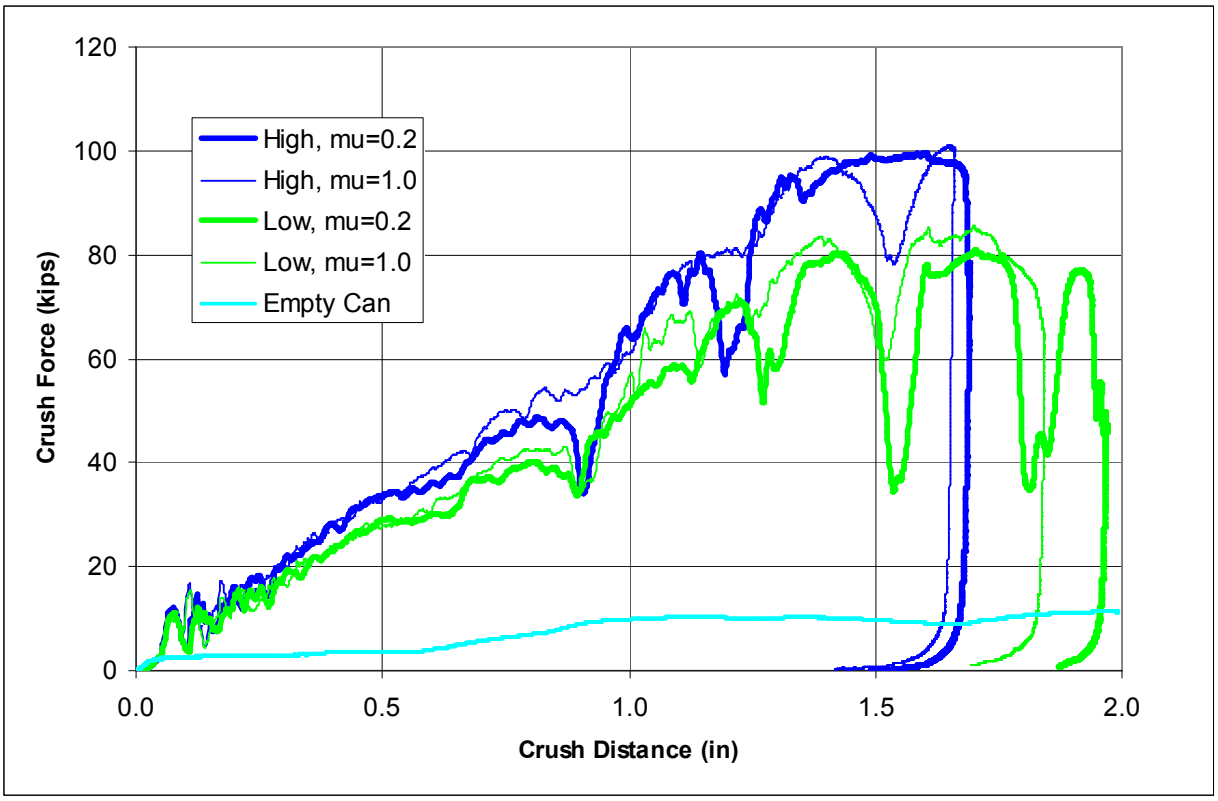

FIGURE 19. HCM PREDICTIONS OF CRUSH FORCE FOR 20^{O} AOA WITH STRENGTH AND FRICTION VARIABILITY

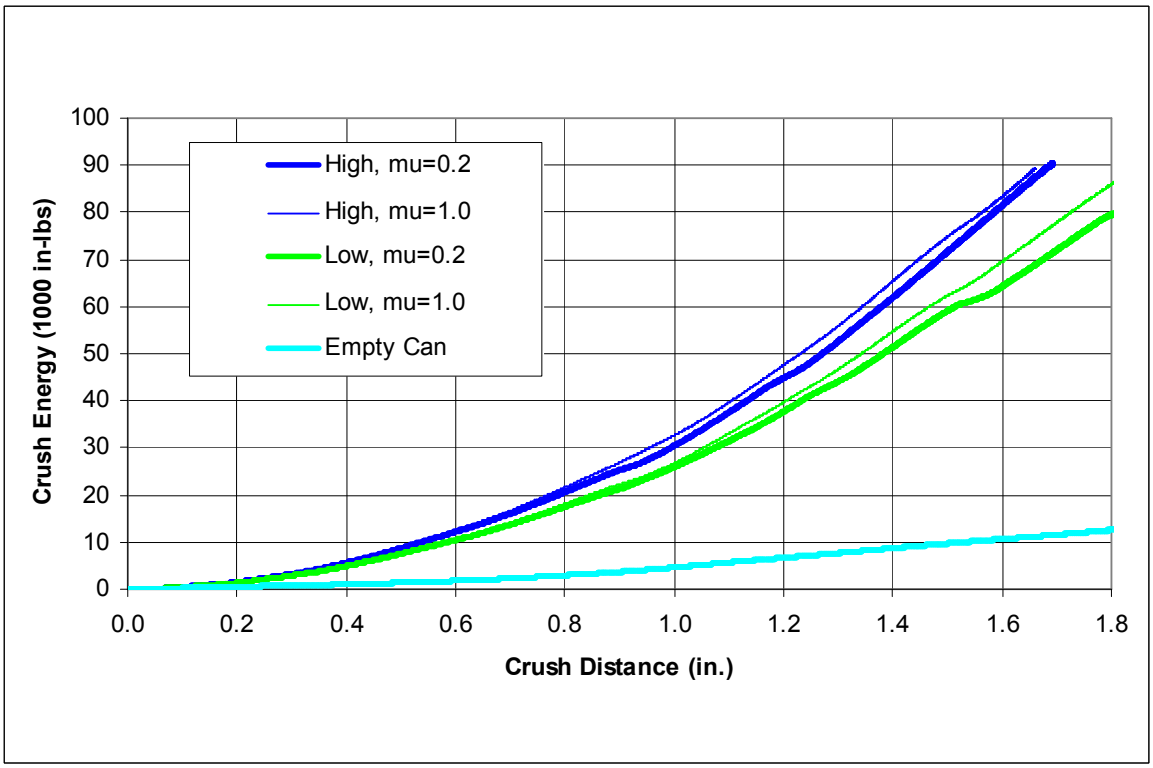

FIGURE 20. HCM PREDICTION OF ENERGY METRIC FOR 20^{O} AOA WITH STRENGTH AND FRICTION VARIABILITY

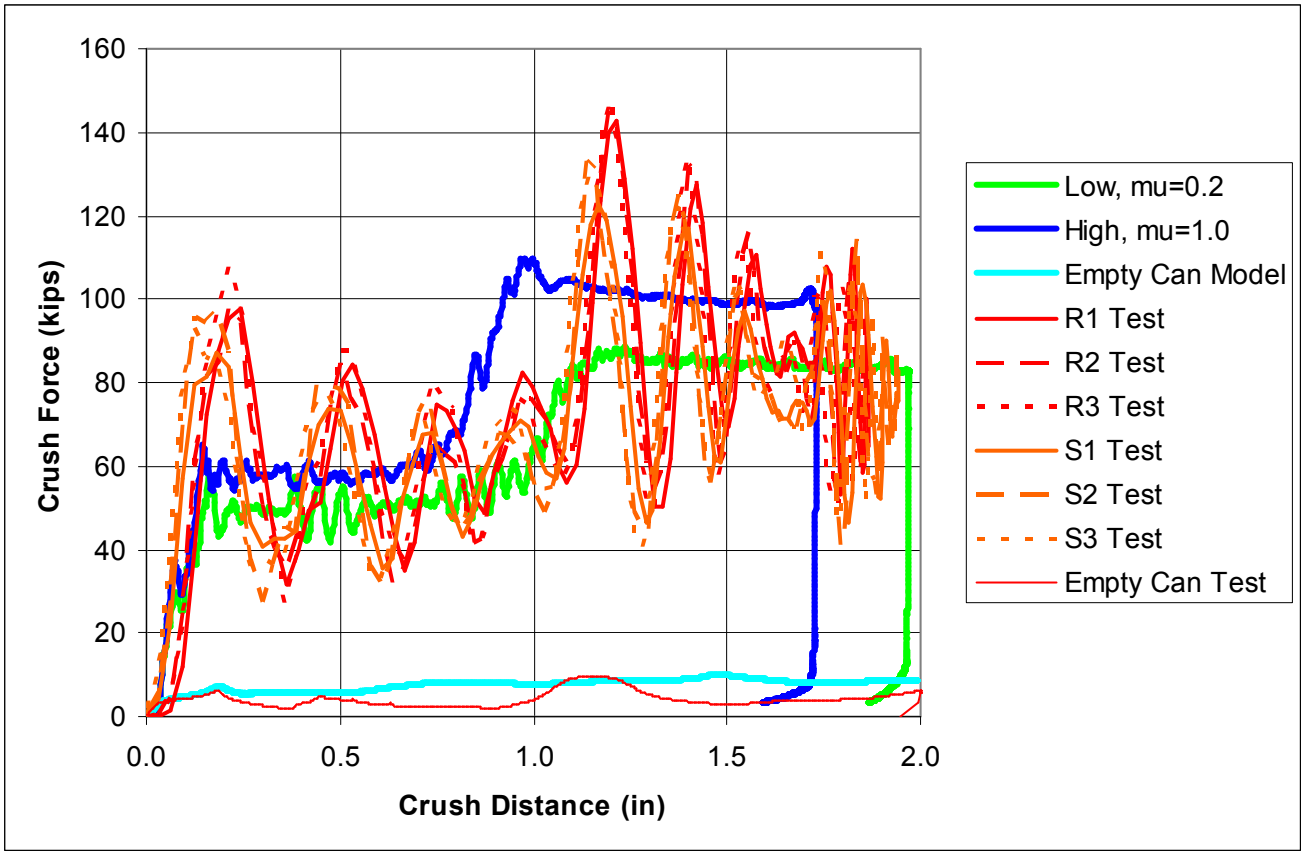

FIGURE 21. HCM PREDICTED RANGE OF CRUSH FORCE FOR 3^{O} AOA COMPARED TO TEST DATA

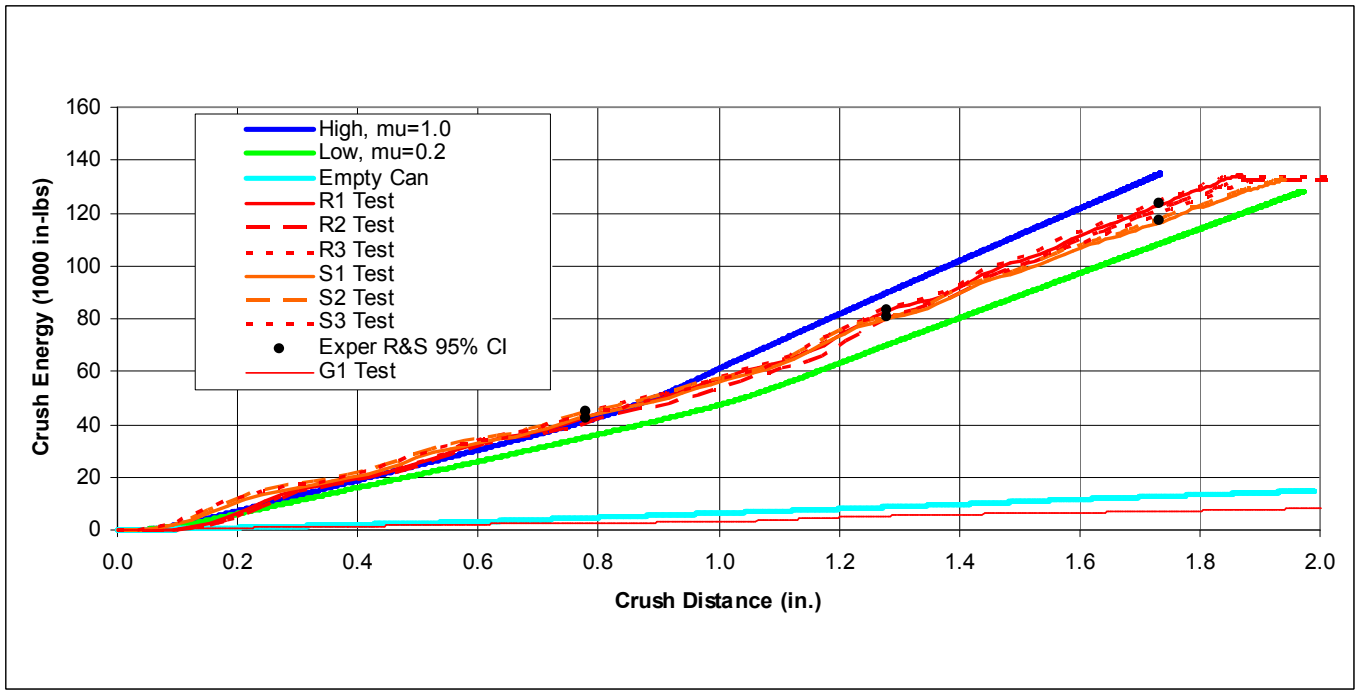

FIGURE 22. HCM PREDICTED RANGE OF ENERGY METRIC FOR 3^{O} AOA COMPARED TO TEST DATA

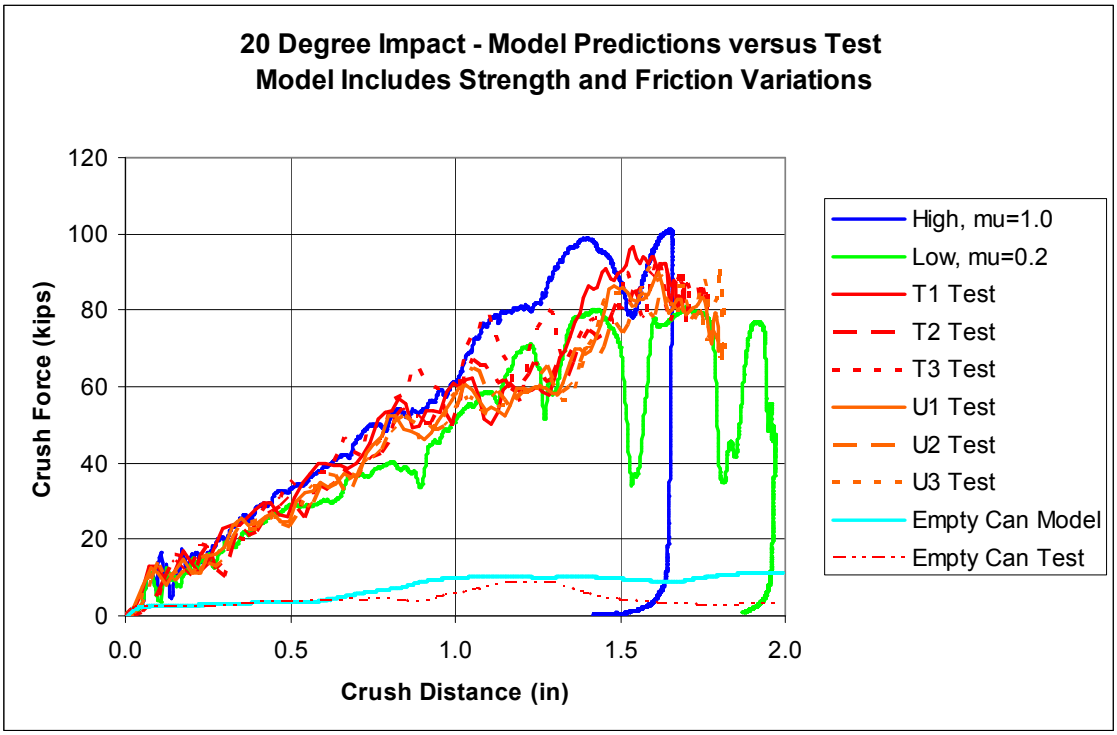

FIGURE 23. HCM PREDICTED RANGE OF CRUSH FORCE FOR 20^{O} AOA COMPARED TO TEST DATA

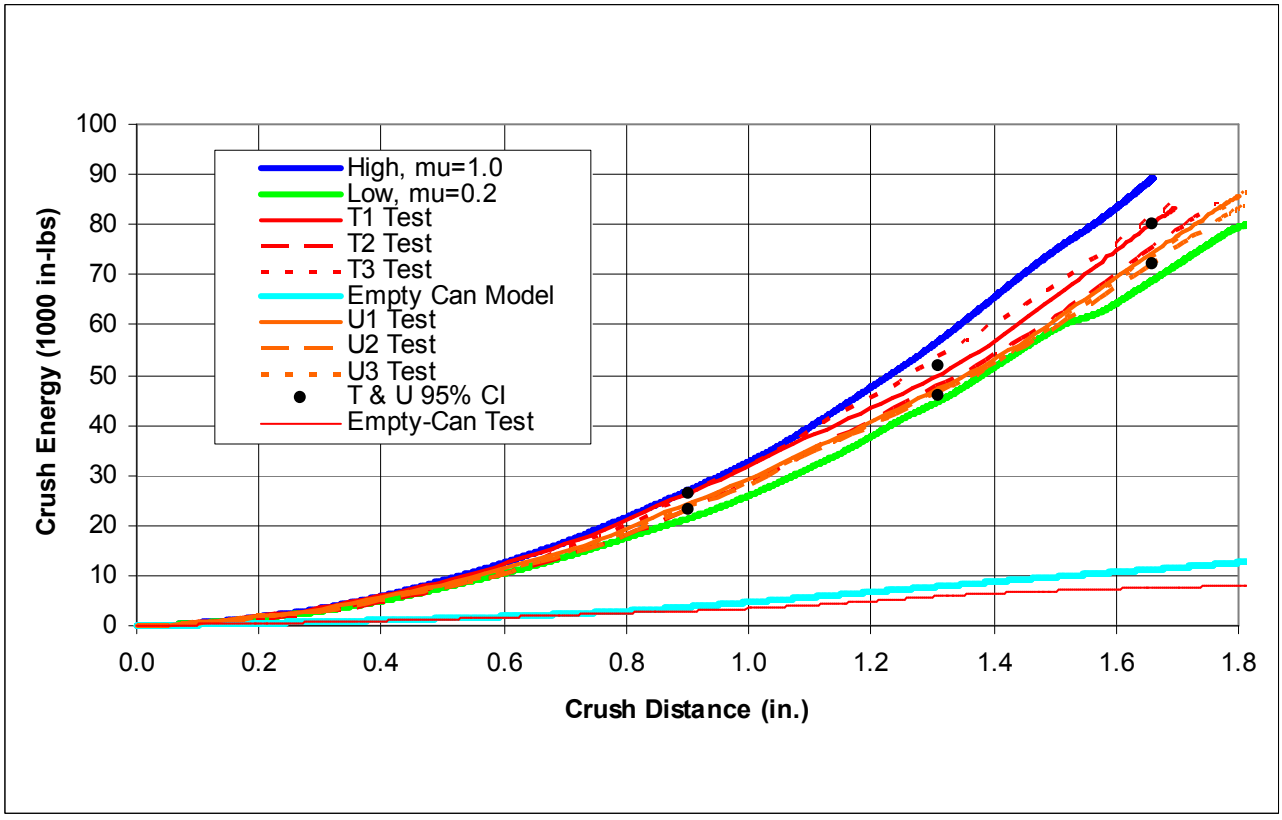

FIGURE 24. HCM PREDICTED RANGE OF ENERGY METRIC FOR 20^{O} AOA COMPARED TO TEST DATA

TABLE 1. HIGH SPEED TESTING RESULTS FROM TECHNIQUE ONE

MTS Material Test Machine Results			
Crush Velocity (in/sec)	Mean Crush Stress (ksi)	Number of Test Samples	95% Confidence Limits
0.0167	5.9	4	0.04
0.75	6	3	0.02
16.95	6.4	3	0.02
160	6.3	6	0.03

TABLE 2. HIGH SPEED TESTING RESULTS FROM TECHNIQUE THREE

Sandia Horizontal Actuator Testing Results		
Sample Name	Mean Crush Rate (ksi)	Mean Crush Stress (Ksi)
V4	377	7.1
V5	517	6.1

TABLE 3. LIST OF RANDOM VARIABLES TO BE PROPAGATED THROUGH THE HCM

Parameter	Value	Description of Parameter
TS (psi)	6100 +/- 10%	Initial strength parameter for TT yield surface
LS (psi)	850+/- 10%	Initial strength parameter for LL yield surface
WS (psi)	600+/-10%	Initial strength parameter for WW yield surface
TLS (psi)	1200 to 1800	Initial strength parameter for TL yield surface
LWS (psi)	300 to 675	Initial strength parameter for LW yield surface
WTS (psi)	700 to 1100	Initial strength parameter for WT yield surface
Friction	0.2 to 1.0	Coulomb friction values

TABLE 4. VALIDATION TEST MATRIX

Quasi-static Test Matrix ~ 0 ft/sec			
Configuration	Temperature deg F	Units	Test Names
3° empty can	T_o	3	G1, 2, 3
20° empty can	T_o	3	H1, 2, 3
3° X on L	T_o	3	J1, 2, 3
20° X on L	T_o	3	K1, 2, 3
20° + on L	T_o	3	L1, 2, 3
20° + on L	165°	3	M1, 2, 3
3° X on L	165°	3	W1, 2, 3
Dynamic Test Matrix ~60-85 ft/sec			
3° X on L	T_o	3	R1, 2, 3
3° X on L	165°	3	S1, 2, 3
20° X on L	T_o	3	T1, 2, 3
20° X on L	165°	3	U1, 2, 3

TABLE 5. MODEL VALIDATION METRICS FOR THE 3^{O} AOA IMPACT

3^{O} AOA Impact Model Validation, 95% Confidence Intervals			
	1/3 E	2/3 E	3/3 E
Crush Distance (in)	0.78	1.28	1.73
Eq. 3, Test 95% C. I., 1000 in-lbs	42.0 to 45.3	80.6 to 83.3	117.1 to 123.7
Nominal Model Value, 1000 in-lbs	38.2	80.2	121.58
Eq. 6, Model Error Estimate, 1000 in-lbs	-3.8 to -7.1	-0.4 to -3.2	-2.1 to 4.5
Eq. 6, Model Error Estimate, %	-8 to -16	-0.5 to -3.8	-1.8 to 3.7

TABLE 6. MODEL VALIDATION METRICS FOR THE 20^{O} AOA IMPACT

20^{O} AOA Impact Model Validation, 95% Confidence Intervals			
	1/3 E	2/3 E	3/3 E
Crush Distance (in)	0.9	1.31	1.66
Eq. 3, Test 95% C. I., 1000 in-lbs	23.3 to 26.19	45.85 to 51.65	72.2 to 80
Nominal Model Value, 1000 in-lbs	24.78	50.95	79.04
Eq. 6, Model Error Estimate, 1000 in-lbs	-1.41 to 1.47	-0.70 to 5.10	-0.94 to 6.87
Eq. 6, Model Error Estimate, %	-5.7 to 5.9	-1.43 to 10.4	-1.23 to 9.04

REFERENCES

1. Lu, W.-Y. and Hinnerichs, T., "Crush of High Density Aluminum Honeycombs," IMECE/AMD-25453, 2001.
2. Lu, W.-Y., Korellis, J., and Hinnerichs, T., "Shear Deformation of High Density Aluminum Honeycombs", IMECE/AMD-44092, 2003
3. Carne, T.G., Neilsen, M.K., and Stasiunas, E.C., "Experimental and Analytical Validation of a Computationally Developed Orthotropic Constitutive Model," Proceedings of IMAC XXI, A Conference on Structural Dynamics, Kissimmee, FL, Feb. 2003.
4. Hinnerichs, T., Neilsen, M. Lu, Wei-Yang, "A New Honeycomb Constitutive Model for Impact Analyses", IMECE2004-60751.
5. Hinnerichs, T.,Lu, Wei-Yang, Field, R., Neilsen, M., "Validation of a Nonlinear Aluminum Honeycomb Constitutive Model for Impact Analyses", Proceedings of the IMAC XXV, A Conference on Structural Dynamics, Kissimmee, FL, Feb. 2005.
6. Lu, Wei-Yang, Korellis, J., Lee, K., Scheffel, S., Hinnerichs, T., Neilsen, M., Scherzinger, W., "Characterization of Aluminum Honeycomb and Experimentation for Model Development and Validation, Volume I: Discovery and Characterization Experiments for High-Density Aluminum Honeycomb", SAND2006-4457, Aug 2006, Sandia National Laboratories, Albuquerque, NM 87185.
7. Hinnerichs, T., Carne, T., Lu, Wei-Yang, Stasiunas, E., Neilsen, M., Scherzinger, W., Rogillio, B., "Characterization of Aluminum Honeycomb and Experimentation for Model Development and Validation, Volume II: Honeycomb Experimentation for Model Development and Validation", SAND2006-4455, Aug 2006, Sandia National Laboratories, Albuquerque, NM 87185.
8. Hinnerichs, T., Pulling, E., Neilsen, M., Lu, Wei-Yang, "Validation of a new aluminum honeycomb constitutive model for impact analyses", IMECE2006-14575, 2006 ASME International Mechanical Engineering Congress & Exposition, Nov 5-10, 2006, Chicago, Ill.
9. Koteras, J.R., Gullerud, A.S., "Presto User's Guide Version 1.05", SAND Report, SAND2003-1089, Sandia National Laboratories, Albuquerque, NM, April 2003.
10. Stasiunas, E., Carne, T., and Rogillio, B., Axial Crush Strength of Tape-Confined and Segmented Honeycomb, Sandia National Laboratories internal memo, Nov 4, 2004.
11. Lu, Wei-Yang, Friction Test Report, internal memo, Sandia National Laboratories, Livermore, CA, May 2006.
12. Baumeister & Marks, *Standard Handbook for Mechanical Engineers*, 7th Edition, McGraw Hill..
13. Devore,J.L.,Probability and Statistics for Engineers and Scientists, 5th ed., Duxbury, Pacific Grove, CA, 2000.
14. Oberkampf, W.L., Barone, M.F., Measures of Agreement Between Computation and Experiment: Validation Metrics, SANDIA REPORT SAND2005-4302, Sandia National Laboratories, Albuquerque, NM 87185, Aug 2005.